COMPEL - The international journal for computation and mathematics in electrical and electronic engineering

Magnetic measurement and analysis of nanocrystalline laminates with different dimensions

Wenbin Meng, Changgeng Zhang and Yongjian Li
State Key Laboratory of Intelligent Power Distribution Equipment and System, Hebei University of Technology, Tianjin, China

He Sun and Qingxin Yang
School of Electrical Engineering and Automation, Tianjin University of Technology, Tianjin, China, and

Pia Lindh
Lappeenranta-Lahti University of Technology, Lappeenranta, Finland

Received 26 January 2026
Revised 3 April 2026
Accepted 30 April 2026

Abstract

Purpose – This paper aims to investigate the influence of geometric dimensions on the macroscopic magnetic properties of nanocrystalline laminates through experimental measurement and analytical interpretation.

Design/methodology/approach – This paper develops a new system for testing the magnetic properties of nanocrystalline laminates with different dimensions and examines seven laminates of two types under various flux densities and excitation frequencies. The effects of geometric parameters, such as length-width ratio and thickness-width ratio, on typical magnetic parameters, including loss density, permeability and coercivity, are investigated through comparative analysis of the experimental data. Furthermore, the established analytical model is used to investigate the nonuniform internal magnetic field intensity distribution in nanocrystalline laminates with different dimensions.

Findings – The results demonstrate that wider laminates exhibit higher loss density, reduced permeability and increased coercivity, with the dimensional influence becoming more pronounced at higher frequencies. Furthermore, the analytical results provide a qualitative explanation for the nonuniform internal magnetic field intensity distribution caused by dimensional variations. Overall, within the investigated dimensional range and excitation conditions of this work, the influence of geometric parameters on the magnetic performance of nanocrystalline laminates tends to increase in the order of thickness, length and width and the effect is frequency-dependent.

Originality/value – This work not only proposes an effective testing method for nanocrystalline laminates of variable dimensions but also provides theoretical and experimental insights for optimizing the design of high-frequency magnetic components.

Keywords Nanocrystalline alloy, Magnetic properties, Laminated sample

Paper type Research paper

1. Introduction

With the development of high-voltage direct current transmission, power equipment requires high power density and low loss. Nanocrystalline soft magnetic alloys, as typical magnetic

Funding: This work was supported in part by the National Natural Science Foundation of China, (No. 52277008, 52130710), Natural Science Foundation of Hebei Province, China (No. E2023202050) and the Funds for Creative Research Groups of Hebei Province, China (No. E2024202298).

Conflict of interest: The authors declare that they have no known competing financial interests or personal relationships that could have appeared to influence the work reported in this paper.

COMPEL - The international journal for computation and mathematics in electrical and electronic engineering
© Emerald Publishing Limited
0332-1649
DOI 10.1108/COMPEL-01-2026-0043

Downloaded from http://www.emerald.com/compel/article-pdf/doi/10.1108/COMPEL-01-2026-0043/11635424/compel-01-2026-0043en.pdf by Zhejiang

materials, exhibit high permeability, high saturation magnetic flux density, low coercivity and a low magnetostriction coefficient, which result in low loss density. They are preferred materials for high-frequency transformers and inductors in energy transmission (Flohrer and Herzer, 2010; Appino *et al.*, 2012; Meng *et al.*, 2025).

As the magnetic flux density distribution of nanocrystalline soft magnetic alloys exhibits significant dependence on shape and size, their macroscopic magnetic properties also vary accordingly (Li *et al.*, 2017). With the trend toward higher frequencies and the miniaturization of magnetic components, the core size has gradually decreased and the nonuniform distribution of magnetic flux density within the material has become increasingly significant (Cui *et al.*, 2013; Loizos *et al.*, 2008; Kefalas and Kladas, 2014). Therefore, it is necessary to investigate the influence of dimensions on the magnetic properties of nanocrystalline soft magnetic alloys. The key to measuring magnetic properties lies in forming a closed magnetic circuit, either intrinsically or by combining the sample with a suitable external magnetic conductor (Zhou, 1994).

The ring sample method inherently forms a closed magnetic circuit, and the magnetic circuit length can be easily determined. It can be combined with the magnetic circuit method to evaluate the magnetic properties of materials (Nakata *et al.*, 1992; Feng *et al.*, 2024; Zhao *et al.*, 2025). Studies on ring-shaped powder core samples of different dimensions have shown that variations in height have no effect on loss density, whereas loss density is sensitive to changes in ring thickness (Saito *et al.*, 2005). Finite element analysis indicates that as the core thickness increases, the magnetic flux density on the outermost side gradually decreases, while that on the innermost side gradually increases (Ishikura *et al.*, 2019). The magnetic circuit method is applied to determine the magnetic flux density distribution in ring and U-shaped cores, yielding a dimension-dependent distribution function that can be incorporated into loss calculations. Compared with the traditional loss calculation method, the calculation accuracy is greatly improved (Agheb and Hoidalen, 2013).

As the winding process of magnetic rings introduces internal stress, the measurement results may deviate from the intrinsic magnetic properties of the material (Beatrice *et al.*, 2016; Zhang *et al.*, 2020). In contrast, open-circuit samples can ensure more uniform magnetization and better reflect the intrinsic magnetic properties of the material. Therefore, single sheet and laminated sheet samples can be measured more accurately (Zhang *et al.*, 2020). At present, the Epstein Frame and the Single Sheet Tester have been widely applied to measure the magnetic properties of electrical steels and amorphous alloys, and the corresponding international standards have been established (IEC 60404–2[S], 1996; Sievert, 2000). However, these methods are mainly suitable for standardized specimens with fixed dimensions, and cannot readily meet the requirements for comparative studies of nanocrystalline laminates with variable geometric parameters, especially under high-frequency excitation. Therefore, a more flexible testing approach is required for magnetic characterization of nanocrystalline laminated samples with different dimensions.

In this paper, a new testing system capable of measuring nanocrystalline laminates of different dimensions is proposed. The tester allows precise control of the distance between the two pole heads, ensuring flexibility in measurement. With this newly designed tester, the magnetic properties of nanocrystalline laminates, including loss density and hysteresis loops, can be accurately obtained. The experimental results are comprehensively analyzed, and the effects of dimension and frequency on the magnetic properties of nanocrystalline soft magnetic alloys are systematically summarized.

2. Versatile magnetic tester

A versatile magnetic property tester is developed for nanocrystalline laminates with different dimensions. The tester uses a C-type yoke with adjustable pole spacing, enabling comparative

Downloaded from http://www.emerald.com/compel/article-pdf/doi/10.1108/COMPEL-01-2026-0043/11635424/compel-01-2026-0043en.pdf by Zhejiang

measurements of laminated samples with different lengths, widths and thicknesses. The orthogonal excitation device forms the core of the test system, and its main magnetic circuit consists of the laminated sample, a C-type magnetic yoke and a pair of laminated cuboid pole heads, as shown in Figure 1(a) and (b). The overall schematic of the tester is shown in Figure 1(c). The pole head has a width of 30 mm. The horizontal distance between the two poles can be adjusted from 60 mm to 170 mm. The lifting platform positions the sample at the center of the pole heads to ensure uniform magnetization. An arbitrary function generator produces the sinusoidal excitation waveform. A power amplifier amplifies the signal to simulate the magnetization state under operating conditions. A voltage probe measures the voltage of the *B* coil. An amplifying circuit is employed to amplify the *H* signal. A digital oscilloscope records voltage and current signals in real time.

As shown in Figure 2, seven nanocrystalline laminated samples with different dimensions are selected and divided into two categories: samples with different length-width ratios and samples with different thickness-width ratios. All laminated samples are prepared from the same batch of 1K107B nanocrystalline ribbon and processed using the same cutting, lamination and testing procedures. Therefore, under the controlled experimental conditions of this study, the observed differences in magnetic properties are mainly attributed to dimensional variations. The specific dimensions of the experimental samples are listed in Table 1, where *l*, *w*, *h* and *s* represent the length, width, thickness and surface area of the laminated samples, respectively.

Finite element analysis is performed on samples of different sizes, and the resulting distribution of magnetic flux density is shown in Figure 3(a). The results indicate that the regions of nonuniformity are mainly located at the junction between the sample and the pole head,

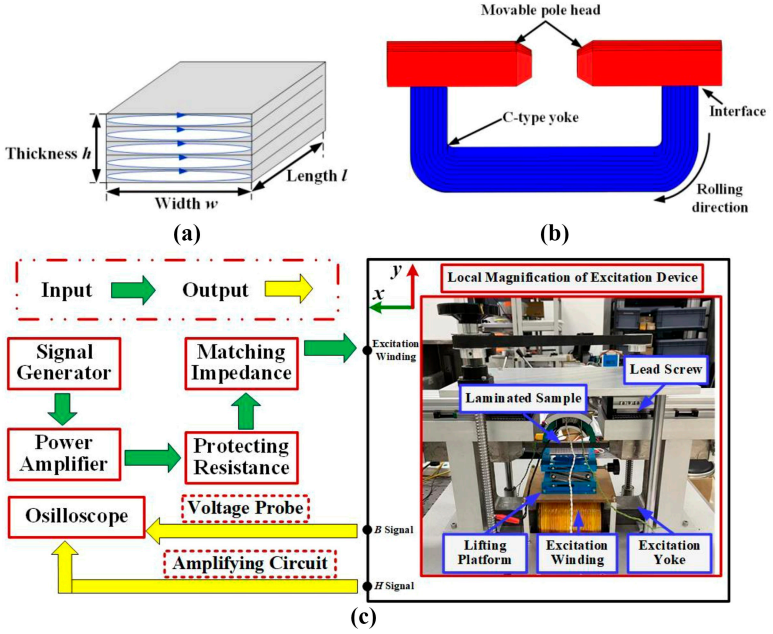
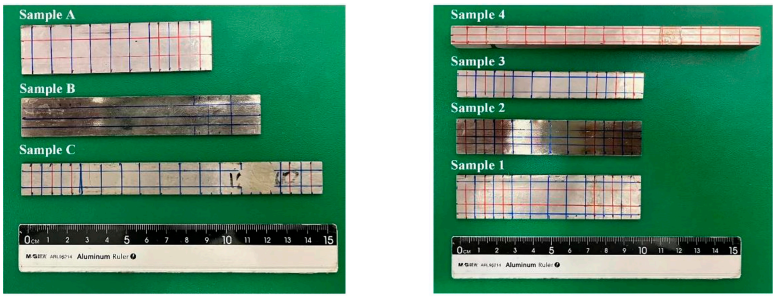


Figure 1. Magnetic properties tester for laminated sample (a) Laminated sample; (b) yoke of excitation; (c) magnetic properties test device diagram

Source: Authors' own work

Downloaded from http://www.emerald.com/compel/article-pdf/doi/10.1108/COMPEL-01-2026-0043/11635424/compel-01-2026-0043en.pdf by Zhejiang



(a) **(b)**

Figure 2. Photos of experimental samples (a) Samples with different length-width ratios; (b) samples with different thickness-width ratios
Source: Authors' own work

Table 1. Geometric dimensions of experimental samples

Sample	w (mm)	h (mm)	l (mm)	s (mm^2)
Sample A	25	2	96	5,284
Sample B	20	2	120	5,360
Sample C	16	2	150	5,464
Sample 1	25	1.5	100	5,357
Sample 2	20	2	100	4,480
Sample 3	15	2.6	100	3,598
Sample 4	10	4	100	2,880

whereas the magnetic flux density remains uniform in the other regions. Furthermore, Figure 3(b) presents the magnetic flux density distribution along the length direction, showing that the magnetic flux density remains uniform over approximately three-quarters of the sample length.

The sensor structure is a key component of the magnetic properties testing system, and it is responsible for collecting the magnetic field signals of the sample. As shown in Figure 4, the B coil and H coil are used to measure the internal flux density and the surface magnetic field intensity of the sample, respectively. The longitudinal and transverse positioning bars shown in Figure 4 fix the position of the sensor coil and ensure experimental repeatability.

For samples with high permeability, the B coil is wrapped around the cuboid sample to improve the accuracy of magnetic flux density measurements, and the magnetic flux density is calculated from the induced electromotive force in the B coil. The H coil is closely attached to the surface of the sample, and the magnetic field intensity is calculated based on Faraday's law of electromagnetic induction and the continuity of the tangential component of the magnetic field, as shown in equation (1):

$$H = \frac{1}{\mu_0 K_{\mathrm{H}}} \int U_{\mathrm{H}} \mathrm{d}t \tag{1}$$

where μ_0 is the vacuum permeability, U_{H} is the induced voltage of the H coil and K_{H} is the calibration coefficient of the H coil, which is obtained from calibration experiments using a long straight solenoid.

Downloaded from http://www.emerald.com/compel/article-pdf/doi/10.1108/COMPEL-01-2026-0043/11635424/compel-01-2026-0043en.pdf by Zhejiang

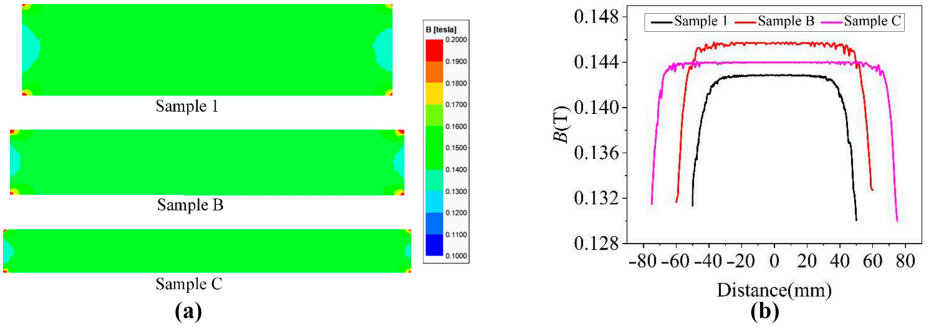


Figure 3. Finite element simulation results of different samples (a) The distribution of magnetic flux density in the sample; (b) magnetic flux density distribution along the length direction
Source: Authors' own work

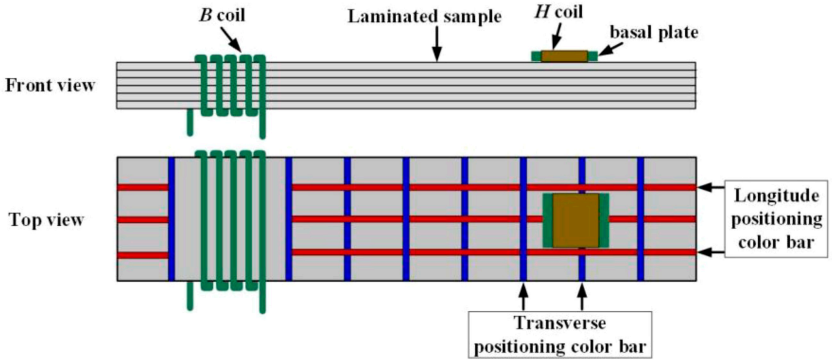


Figure 4. Schematic diagram of *B-H* sensing coil
Source: Authors' own work

The analytical expression for the magnetic flux density at the center of the axis of a long straight solenoid is given as:

$$B(t) = \mu_0 H(t) = \left(\mu_0 N_{01} i(t) \cos\theta\right) / l_{01} \tag{2}$$

where N_{01} is the number of turns of the solenoid, l_{01} is the length of the solenoid, $i(t)$ is the instantaneous value of the sinusoidal excitation current and θ is the angle between the radial direction of the solenoid and the axis of the sample support platform, with the cosine expression given by:

$$\cos\theta = \frac{l_{01}}{2\sqrt{r_c{}^2 + (l_{01}/2)^2}} \tag{3}$$

where r_c is the radius of the solenoid.

Downloaded from http://www.emerald.com/compel/article-pdf/doi/10.1108/COMPEL-01-2026-0043/11635424/compel-01-2026-0043en.pdf by Zhejiang

According to Faraday's law of electromagnetic induction:

$$U = K_H \frac{\mathrm{d}B(t)}{\mathrm{d}t} \tag{4}$$

where U is the effective value of the induced voltage in the sensing H coil, and $B(t)$ is the magnetic flux density through the sensing coil.

Finally, the coefficient K_H of the H sensing coil is given in equation (5):

$$K_H = \frac{U}{2\pi f B} \tag{5}$$

Substituting the H coil calibration data into equation (5) yields the calibration coefficients at different excitation frequencies. The calibration results obtained at 50 and 100 Hz are presented in Table 2. The corresponding average values, 1.312056 and 1.320416, are in good agreement, indicating that the variation in K_H is small under the calibration conditions adopted in this study. Such variation is mainly attributed to measurement uncertainty, including instrument accuracy, reading dispersion and installation errors. Therefore, the average value of 1.316 is used as the final calibration coefficient K_H.

3. Experimental analysis of laminated samples

Based on the magnetic tester shown in Figure 1, the magnetic properties of laminated samples with different dimensions are measured under sinusoidal excitation. The excitation frequency ranges from 1 kHz to 15 kHz, and the magnetic flux density varies from 0.1T to 0.6T. Under the same testing conditions, the magnetic properties of samples with different dimensions are compared.

Figure 5 shows the alternating hysteresis loops of samples with different length-width ratios at excitation frequencies of 1 kHz and 15 kHz. The hysteresis loops of samples with different length-width ratios exhibit similar shapes, all of which are approximately ellipsoidal. For samples with a smaller length-width ratio (i.e. wider samples), a higher magnetic field intensity is required to reach the same magnetic flux density, and the area enclosed by the hysteresis loop is larger. At f = 1 kHz, both sample A and sample C are magnetized to 0.6T. However, sample C (with a smaller width) requires only 50A/m, compared with 80A/m for sample A.

Figure 6 shows the hysteresis loops of samples with different thickness–width ratios at excitation frequencies of 1 kHz and 15 kHz. Similarly, samples with a smaller thickness-width ratio in the present sample set exhibit larger remanence and are more difficult to magnetize.

Table 2. *H* coil calibration coefficients at different frequencies

Current (A)	Induced voltage 50Hz (mV)	Induced voltage 100Hz (mV)	Calibration coefficient 50Hz (10^{-3}m^2)	Calibration coefficient 100Hz (10^{-3}m^2)
1.0	0.6	1.22	1.303995	1.325728
2.0	1.22	2.43	1.325728	1.320295
3.0	1.82	3.65	1.318484	1.322106
4.0	2.41	4.84	1.309428	1.318157
5.0	3.02	6.07	1.312688	1.319208
6.0	3.61	7.29	1.302191	1.317002

Downloaded from http://www.emerald.com/compel/article-pdf/doi/10.1108/COMPEL-01-2026-0043/11635424/compel-01-2026-0043en.pdf by Zhejiang

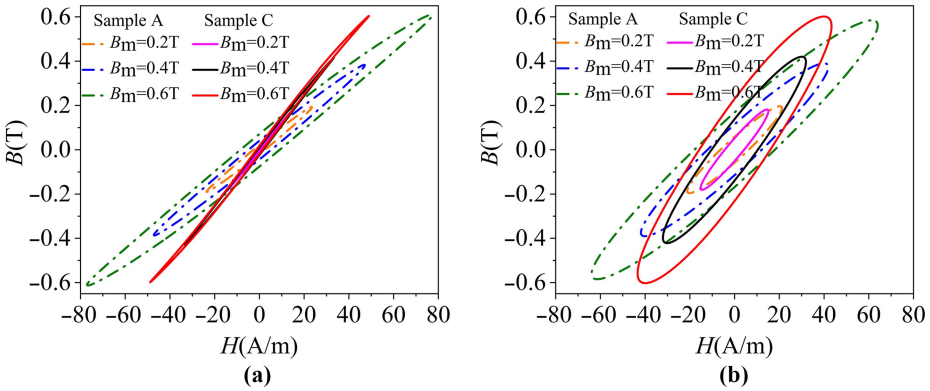


Figure 5. Hysteresis loops of samples with different length-width ratios and frequencies (a) 1 kHz; (b) 15 kHz

Source: Authors' own work

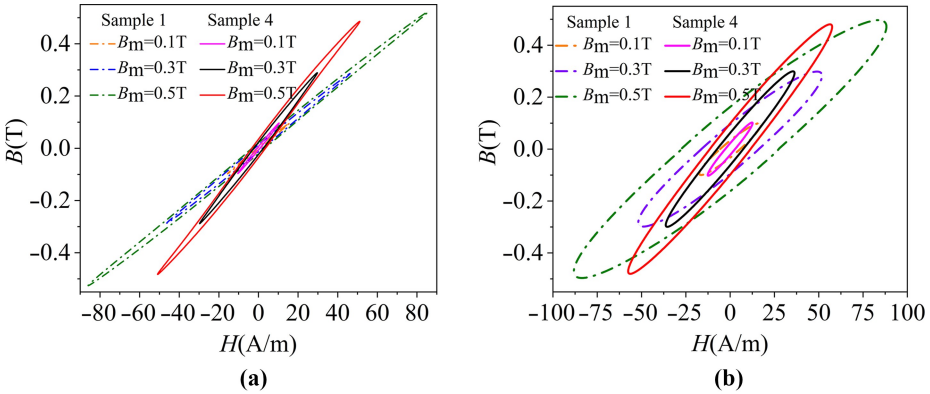


Figure 6. Hysteresis loops of samples with different thickness-width ratios and frequencies (a) 1 kHz; (b) 15 kHz

Source: Authors' own work

Figure 7(a) and (b) compare the loss densities of samples with different length-width ratios. At the same frequency and magnetic flux density, wider samples exhibit slightly higher loss density than narrower samples. Moreover, the difference in loss density between samples of different dimensions becomes more pronounced at higher flux densities. Figure 7(c) and (d) show the loss densities of samples with different thickness-width ratios. Similarly, samples with a smaller thickness-width ratio exhibit higher loss densities.

The magnetization characteristics of samples with different dimensions are presented in Figure 8. In Figure 8(a), the slopes of the magnetization curves represent the permeability of the nanocrystalline laminates. The slopes of the magnetization curves decrease as the sample width increases, reflecting a reduction in permeability. Figure 8(b) shows that as the width increases, the coercivity of the laminated samples also increases. Therefore, it can be concluded that wider samples are more difficult to magnetize.

Downloaded from http://www.emerald.com/compel/article-pdf/doi/10.1108/COMPEL-01-2026-0043/11635424/compel-01-2026-0043en.pdf by Zhejiang

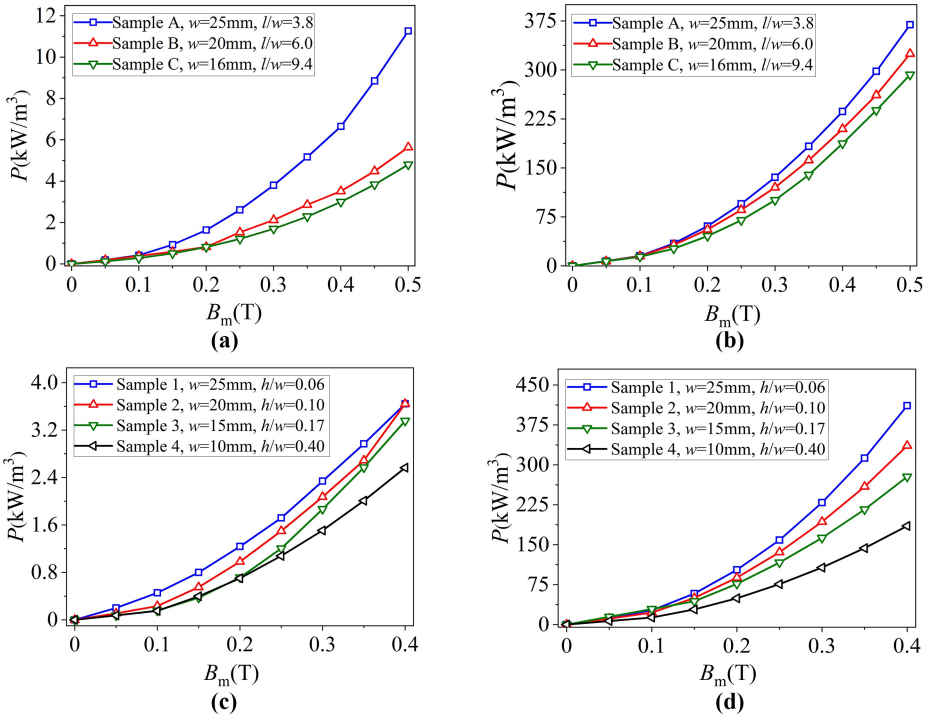


Figure 7. Measurement results of samples with different dimensions and frequencies (a) Different length-width ratios, $f = 1$ kHz; (b) different length-width ratios, $f = 15$ kHz; (c) different thickness-width ratios, $f = 1$ kHz; (d) different thickness-width ratios, $f = 15$ kHz

Source: Authors' own work

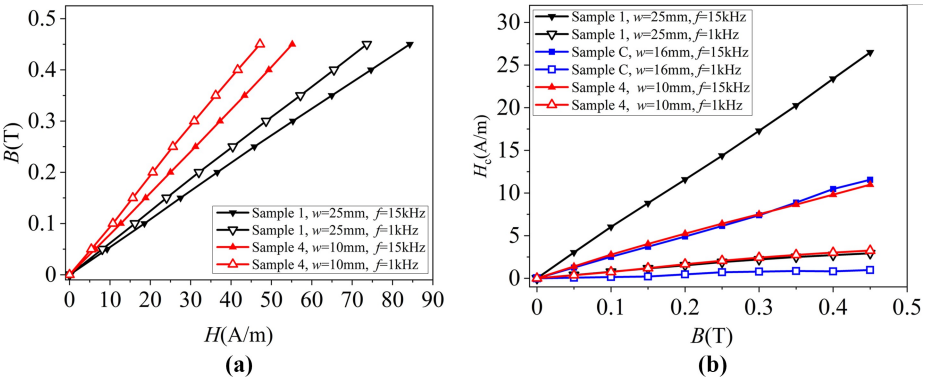


Figure 8. Magnetization characteristics comparison between samples with different geometric dimensions (a) Magnetization curves; (b) unsaturated coercivities

Source: Authors' own work

Downloaded from http://www.emerald.com/compel/article-pdf/doi/10.1108/COMPEL-01-2026-0043/11635424/compel-01-2026-0043en.pdf by Zhejiang

4. Effect of geometric dimension on magnetic field intensity distribution

The above experimental results show that the magnetic properties of nanocrystalline laminates are directly related to the length–width ratio and the thickness–width ratio of the samples. Within the investigated dimensional range and experimental conditions of this work, the influence of geometric parameters on the magnetic properties of the samples tends to increase in the order of thickness, length and width. The thickness of the laminated sample has the least effect on its magnetic properties, which reflects the good insulation between the sheets in the laminate. Therefore, for qualitative analysis, the single sheet model can be extended to laminated samples to simplify the discussion. The distribution of magnetic field intensity in a single sheet is studied to explain the relationship between macroscopic magnetic properties and sample dimensions. The dimensions of a single sheet are shown in Figure 9. The analysis in this section is mainly intended to provide a qualitative physical interpretation of the experimentally observed dimensional dependence, rather than a strict quantitative prediction of loss, permeability, or coercivity.

The influence of sample dimensions on the magnetic field distribution of a rectangular sheet placed in an external magnetic field is quantitatively analyzed. Owing to the demagnetization effect of eddy currents, the magnetic field intensity in the *xoy* plane gradually decreases from the boundary toward the center. When the sample width is much larger than its thickness, the sample can be approximated as a single sheet of infinite width and the distribution of magnetic field intensity along the *x* direction is expressed as (Howard and Kazimierczuk, 2001):

$$|H(x)| = H_{01}\sqrt{\frac{\cosh(2(\gamma/d)(x-d/2)) + \cos(2(\gamma/d)(x-d/2))}{\cosh(\gamma) + \cos(\gamma)}} \tag{6}$$

$$\gamma = \sqrt{\pi\sigma\mu d^2 f} \tag{7}$$

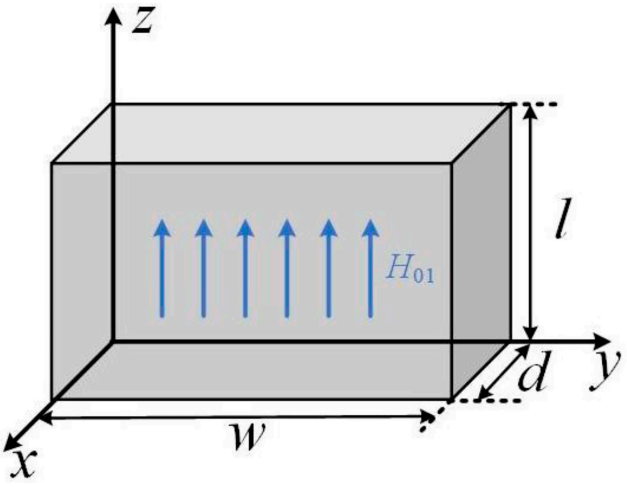


Figure 9. A single sheet sample placed in external magnetic field
Source: Authors' own work

Downloaded from http://www.emerald.com/compel/article-pdf/doi/10.1108/COMPEL-01-2026-0043/11635424/compel-01-2026-0043en.pdf by Zhejiang

where $H(x)$ represents the distribution function of magnetic field intensity along the thickness direction, H_{01} is the applied magnetic field intensity along the length of the single sheet, σ is the conductivity of the nanocrystalline soft magnetic alloy, μ is the permeability of the nanocrystalline soft magnetic alloy and d is the thickness of the single sheet material.

When the sample width w is not much larger than the thickness d, the double Fourier sine transform is used to solve Maxwell's equations, yielding an analytical expression for the magnetic field intensity within the sheet in the form of a double series:

$$H(x,y)=\left[H_{01}-\sum_{m=1,3\ldots}^{\infty}\sum_{n=1,3\ldots}^{\infty}K_{mn}\sin(p_m x)\sin(q_n y)\right] \tag{8}$$

$$\begin{cases} p_m = m\pi/d \\ q_n = n\pi/w \\ K_{\mathrm{mn}} = (16\upsilon^2 H_{01})/\left(mn\pi^2\left(\upsilon^2+p_m^2+q_n^2\right)\right) \\ \upsilon = (1+j)\gamma/d \end{cases} \tag{9}$$

where $H(x, y)$ represents the distribution function of magnetic field intensity in the entire xoy plane.

The magnetic field intensity distribution within a single sheet of the same size is obtained from equations (6) and (8), as shown in Figure 10. When the sample is approximated as a single sheet of infinite width, the magnetic field intensity distribution exhibits a "U" shape, which is nonlinear only in the thickness direction. The magnetic field intensity distribution obtained from equation (8) exhibits a "chamfered table" shape, with the surface magnetic field intensity gradually decreasing from the edges toward the center. This indicates that for a finite-width sample, the distribution of magnetic field intensity along the width direction near the edges resembles that along the length direction, and a peak value also appears. If the

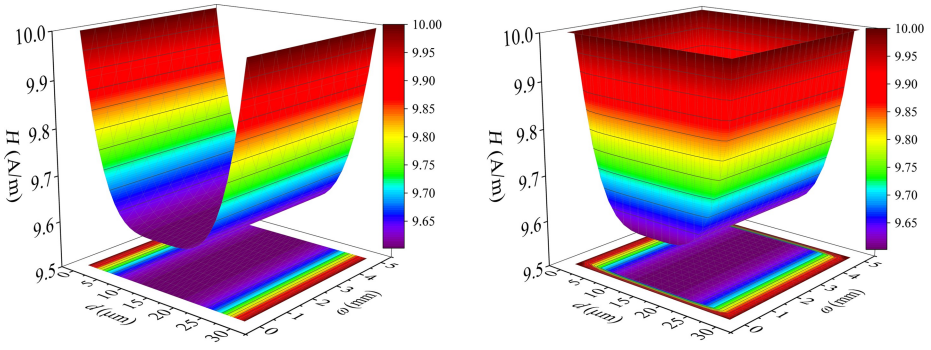


Figure 10. Distribution of magnetic field intensity in the xoy plane of a sheet sample (a) Magnetic field intensity distribution in an infinite-width single sheet; (b) magnetic field intensity distribution in a finite-width single sheet

Source: Authors' own work

Downloaded from http://www.emerald.com/compel/article-pdf/doi/10.1108/COMPEL-01-2026-0043/11635424/compel-01-2026-0043en.pdf by Zhejiang

sample is approximated as a single sheet of infinite width, the core loss calculated from equation (6) yields significant errors due to the oversimplified field distribution.

Equation (8) is used to obtain the magnetic field intensity distribution in single sheets with different thickness-width ratios, as shown in Figure 11. The parameters for the single-sheet calculations are set as follows: the thickness of a single sheet d is 2 mm; The width w is 2 and 8 mm, respectively; the relative permeability is 8×10^4; the conductivity is 8.3×10^5 S/m; the frequency is 1 kHz. Figure 11 shows that the minimum magnetic field intensity always occurs at the center of the sample. As the sample width increases, the distribution of magnetic field intensity in the thickness direction remains unchanged, whereas the skin depth in the width direction increases. Therefore, changes in sample dimension make the internal magnetic field intensity distribution nonuniform, which in turn alters the macroscopic magnetic properties of the material.

The above analysis mainly focuses on the effect of geometric dimensions on the magnetic field intensity distribution inside the sheet. In addition to geometric factors, electromagnetic parameters such as relative permeability and excitation frequency also affect the internal

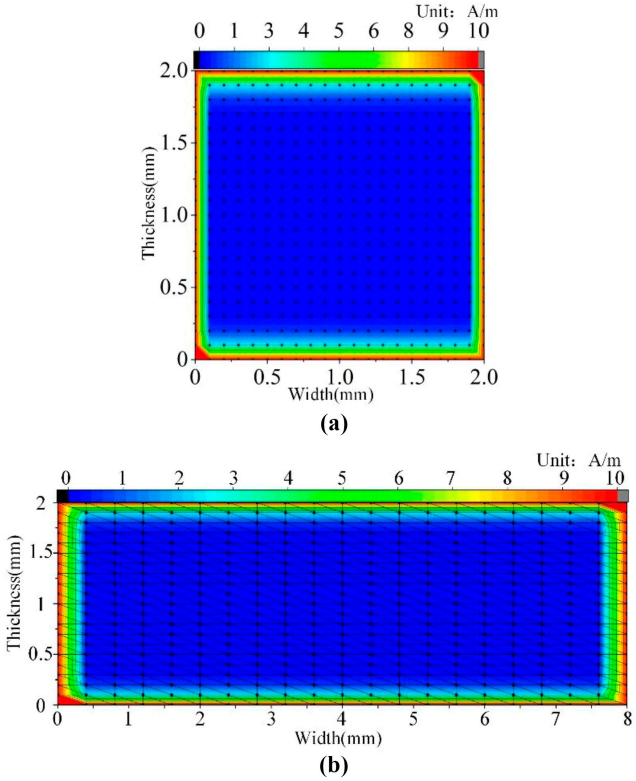


Figure 11. Distribution of magnetic field intensity in the *xoy* plane of a sheet sample (a) Magnetic field intensity distribution of a single sheet with a thickness-width ratio of 1; (b) magnetic field intensity distribution of a single sheet with a thickness-width ratio of 0.25

Source: Authors' own work

Downloaded from http://www.emerald.com/compel/article-pdf/doi/10.1108/COMPEL-01-2026-0043/11635424/compel-01-2026-0043en.pdf by Zhejiang

magnetic field intensity distribution. To investigate the effect of relative permeability on the magnetic field intensity distribution, the thickness d and width w are set to 0.03 and 30 mm, respectively. The relative permeability is taken as 10,000, 40,000, 80,000 and 100,000, while the electrical conductivity and frequency are fixed at 833333 S/m and 10 kHz, respectively. Figure 12 presents the distribution curves of magnetic field intensity along the thickness and width directions of the sample. As the relative permeability increases, the skin effect of the magnetic field within the sheet becomes more pronounced, and the ratio of the skin depths in the thickness and width directions gradually becomes smaller than the thickness-width ratio of the sample.

To investigate the effect of excitation frequency on the magnetic field intensity distribution, the thickness *d* and width *w* are set to 0.03 and 30 mm, respectively. The relative permeability is fixed at 80,000, and the electrical conductivity is set to 833333 S/m. The excitation frequency is taken as 1 kHz, 5 kHz, 10 kHz and 15 kHz. Figure 13 shows the distribution curves of the

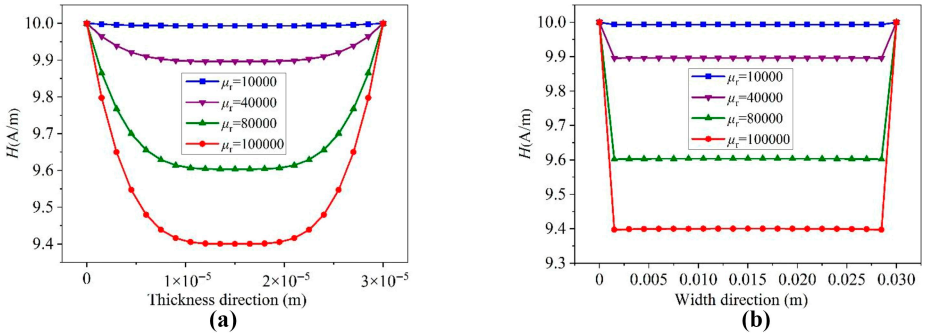


Figure 12. Distribution of magnetic field intensity in a sheet sample with different relative permeability (a) Magnetic field intensity distribution along the thickness direction; (b) magnetic field intensity distribution along the width direction

Source: Authors' own work

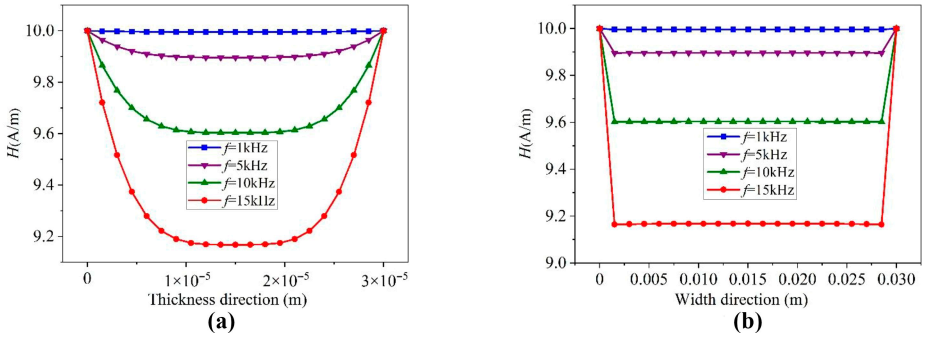


Figure 13. Distribution of magnetic field intensity in a sheet sample at different frequencies (a) Magnetic field intensity distribution along the thickness direction; (b) magnetic field intensity distribution along the width direction

Source: Authors' own work

Downloaded from http://www.emerald.com/compel/article-pdf/doi/10.1108/COMPEL-01-2026-0043/11635424/compel-01-2026-0043en.pdf by Zhejiang

magnetic field intensity along the thickness and width directions of the sample under different excitation frequencies. It can be seen that, as the excitation frequency increases, the skin effect of the magnetic field intensity within the sheet becomes more pronounced.

In summary, geometric dimensions strongly affect the internal magnetic field intensity distribution of laminated samples. For finite-width samples, edge effects lead to a gradual decrease in magnetic field intensity from the edges toward the center, resulting in a nonuniform distribution. Relative permeability and excitation frequency further modify this distribution by enhancing the skin effect. Therefore, the observed differences in macroscopic magnetic properties can be understood as the result of geometry-dominated changes in internal magnetic field intensity distribution, further influenced by material parameters and excitation conditions.

5. Conclusion

A versatile magnetic property tester is developed to evaluate nanocrystalline laminates with variable dimensions, enabling precise measurements under sinusoidal excitation. Tests are conducted on seven laminates with different length-width and thickness-width ratios, within a magnetic flux density range of 0.1–0.6T and a frequency range of 1–15 kHz. The results demonstrate that wider laminates exhibit higher loss density, lower permeability and larger coercivity, with dimensional effects becoming more significant at higher frequencies. For the 1K107B nanocrystalline laminates investigated in this work, within the studied dimensional range and excitation conditions, the influence of geometric parameters tends to increase in the order of thickness, length and width. The analytical results further indicate that dimensional variations lead to a nonuniform internal magnetic field intensity distribution, and that this distribution is further affected by relative permeability and excitation frequency. These results provide useful guidance for the magnetic characterization and structural design of nanocrystalline materials in high-frequency transformers and inductors.

References

Agheb, E. and Hoidalen, H.K. (2013), "Modification of empirical core loss calculation methods including flux distribution", *IET Electric Power Applications*, Vol. 7 No. 5, pp. 381-390, doi: 10.1049/iet-epa.2012.0368.

Appino, C., Bottauscio, O., de La Barrière, O., Fiorillo, F., Manzin, A. and Ragusa, C. (2012), "Computation of eddy current losses in soft magnetic composites", *IEEE Transactions on Magnetics*, Vol. 48 No. 11, pp. 3470-3473, doi: 10.1109/TMAG.2012.2205670.

Beatrice, C., Dobák, S., Ferrara, E., Fiorillo, F., Ragusa, C., Fuzer, J. and Kollar, P. (2016), "Broadband magnetic losses of nanocrystalline ribbons and powder cores", *Journal of Magnetism and Magnetic Materials*, Vol. 420 No. 1, pp. 317-323, doi: 10.1016/j.jmmm.2016.07.045.

Cui, H., Ngo, K.D.T., Moss, J., Lim, M.H.F. and Rey, E. (2013), "Inductor geometry with improved energy density", *IEEE Transactions on Power Electronics*, Vol. 29 No. 10, pp. 5446-5453, doi: 10.1109/TPEL.2013.2289926.

Feng, C., Zhang, Y. and Chi, Q. (2024), "Design of a novel rotary transformer with accurate prediction of nanocrystalline soft magnetic alloy core loss using improved Steinmetz formulation", *IEEE Transactions on Industry Applications*, Vol. 60 No. 2, pp. 2764-2772, doi: 10.1109/TIA.2023.3348776.

Flohrer, S. and Herzer, G. (2010), "Random and uniform anisotropy in soft magnetic nanocrystalline soft magnetic alloys (invited)", *Journal of Magnetism and Magnetic Materials*, Vol. 322 Nos 9-12, pp. 1511-1514, doi: 10.1016/j.jmmm.2009.07.087.

Downloaded from http://www.emerald.com/compel/article-pdf/doi/10.1108/COMPEL-01-2026-0043/11635424/compel-01-2026-0043en.pdf by Zhejiang

Howard, K. and Kazimierczuk, M.K. (2001), "Eddy-current power loss in laminated iron cores", *IEEE International Symposium on Circuits and Systems*, Vol. 3 No. 2, pp. 668-671, doi: 10.1109/ISCAS.2001.921399.

International Electrotechnical Commission (1996), *Magnetic materials—part 2: methods of measurement of the magnetic properties of electrical steel sheet and strip by means of an Epstein frame: IEC Standard, 60402-2*.

Ishikura, Y., Imaoka, J., Noah, M. and Yamamoto, M. (2019), "An improved core loss calculation method considering the non-uniform distribution of magnetic flux density in powder cores", *IET Power Electronics*, Vol. 12 No. 6, pp. 1393-1399, doi: 10.1049/iet-pel.2018.5362.

Kefalas, T.D. and Kladas, A.G. (2014), "Reduction of cost and losses of transformers by using composite magnetic cores", *International Conference on Electrical Machines IEEE*, pp. 2257-2263, doi: 10.1109/ICELMACH.2014.6960499

Li, Z., Yao, K., Li, D., Ni, X. and Lu, Z. (2017), "Core loss analysis of finemet type nanocrystalline soft magnetic alloy ribbon with different thickness", *Progress in Natural Science: Materials International*, Vol. 27 No. 5, pp. 588-592, doi: 10.1016/j.pnsc.2017.09.002.

Loizos, G., Kefalas, T., Kladas, A., Souflaris, T. and Paparigas, D. (2008), "Flux distribution in single phase, Si-Fe, wound transformer cores", *Journal of Magnetism and Magnetic Materials*, Vol. 320 No. 20, pp. e874-e877, doi: 10.1016/j.jmmm.2008.04.068.

Meng, W., Zhang, C., Li, Y. and Zhang, H. (2025), "Comparison of micromagnetic modeling and experiment considering grain size distribution at 1–20kHz", *Journal of Magnetism and Magnetic Materials*, Vol. 629 No. 1, p. 173350, doi: 10.1016/j.jmmm.2025.173350.

Nakata, T., Takahashi, N., Fujiwara, K., Nakano, M., Ogura, Y. and Matsubara, K. (1992), "An improved method for determining the DC magnetization curve using a ring specimen", *IEEE Transactions on Magnetics*, Vol. 28 No. 5, pp. 2456-2458, doi: 10.1109/20.179524.

Saito, T., Takemoto, S. and Iriyama, T. (2005), "Resistivity and core size dependencies of eddy current loss for Fe-Si compressed cores", *IEEE Transactions on Magnetics*, Vol. 41 No. 10, pp. 3301-3303, doi: 10.1109/TMAG.2005.854905.

Sievert, J. (2000), "The measurement of magnetic properties of electrical sheet steel survey on methods and situation of standards", *Journal of Magnetism and Magnetic Materials*, Vols 215-216 No. 1, pp. 647-651, doi: 10.1016/S0304-8853(00)00251-1.

Zhang, X., Li, L., Zhang, Y. and Pang, J. (2020), "Magnetic measurement of nanocrystalline soft magnetic alloy based on a single sheet tester", *IET Science, Measurement and Technology*, Vol. 15 No. 1, pp. 85-93, doi: 10.1049/smt2.12011.

Zhao, X., Zhu, W., Miao, Y., Zuo, S. and Gao, S. (2025), "A dynamic hysteresis model considering the eddy current field inside the metal particle from a microscopic perspective", *Journal of Magnetism and Magnetic Materials*, Vol. 630 No. 15, p. 173387, doi: 10.1016/j.jmmm.2025.173387.

Zhou, S. (1994), *Magnetic Measurement*, Publishing House of Electronics Industry, Beijing.

Further reading

Zhang, L., Wang, Y., Zou, L., Guo, K., Li, Y. and Sun, Q. (2023), "Effect of grain size on magnetic loss of nanocrystalline soft magnetic alloy under High-Frequency Non-Sinusoidal excitation", *IEEE Transactions on Magnetics*, Vol. 59 No. 7, pp. 1-11, doi: 10.1109/TMAG.2023.3277075.

Corresponding author

Changgeng Zhang can be contacted at: changgeng.zhang@hebut.edu.cn

For instructions on how to order reprints of this article, please visit our website:
www.emeraldgrouppublishing.com/licensing/reprints.htm
Or contact us for further details: **permissions@emeraldinsight.com**

Downloaded from http://www.emerald.com/compel/article-pdf/doi/10.1108/COMPEL-01-2026-0043/11635424/compel-01-2026-0043en.pdf by Zhejiang